

# Experimental and computational studies on tritium permeation mechanism in erbium oxide

Wei Mao<sup>1),\*</sup>, Takumi Chikada<sup>1)</sup>, Akihiro Suzuki<sup>2)</sup>, Takayuki Terai<sup>1)</sup> and Kenji Yamaguchi<sup>3)</sup>

1) *Department of Nuclear Engineering and Management, School of Engineering, The University of Tokyo, 7-3-1 Hongo, Bunkyo-ku, Tokyo 113-8656, Japan.*

2) *Nuclear Professional School, School of Engineering, The University of Tokyo, 2-22, Shirakata-shirane, Tokai, Naka, Ibaraki 319-1188, Japan.*

3) *Quantum Beam Science Directorate, Japan Atomic Energy Agency, 2-4 Shirakata-shirane, Tokai, Naka, Ibaraki 319-1195, Japan.*

(Received: 10 May 2012 / Accepted: 3 October 2012)

A tritium permeation barrier (TPB) is much required in fusion blankets to reduce the loss of fuel and minimize radiological hazard. However, the detailed mechanism of tritium permeation through TPB coatings has not yet been clarified because of their complicated crystal structures. To understand the microscopic mechanism, we have not only prepared and characterized nanostructured ceramic  $\text{Er}_2\text{O}_3$  thin films, but also studied the energetics and mobility of interstitial deuterium in cubic bulk  $\text{Er}_2\text{O}_3$  using *ab initio* density-functional calculations. The estimated diffusion activation energy ( $E_a$ ) of interstitial deuterium is somewhat higher than the diffusion energy barrier observed experimentally at 873 K. This result shows that grain boundary structures existing in the TPB of  $\text{Er}_2\text{O}_3$  significantly lower the diffusion barrier and change the diffusion pathway. Transport of hydrogen and its isotopes through the  $\text{Er}_2\text{O}_3$  coatings are likely to be dominated by grain boundaries rather than by grains.

Keywords: Hydrogen isotope permeation measurement, Erbium oxide, Density functional theory calculations, Nudged elastic band

## 1. Introduction

There is no doubt that the environmental and economic acceptability of presently conceived D-T fueled fusion power plants will be dependent on the ability to contain and handle tritium within the reactor building and to control tritium releases to the environment without incurring into exorbitant costs [1, 2]. The problems of tritium leakage have been studied since 1970's [3], and tritium permeation barrier (TPB) coating has been one of the most important subjects in the development of liquid lithium blanket for fusion systems. As to coating materials, a great many ceramics such as  $\text{Y}_3\text{Al}_2\text{O}_{12}$ , CaO, MgO, AlN (aluminum nitride),  $\text{Al}_2\text{O}_3$ ,  $\text{Y}_2\text{O}_3$  and  $\text{Er}_2\text{O}_3$  were initially considered potentially eligible. Of these  $\text{Er}_2\text{O}_3$  was selected as one of the most preferable candidate materials for TPB coatings because of its high permeation reduction factor (PRF) [4], high thermodynamic stability at high temperatures and in air, good compatibility with liquid Li, and high electrical resistivity [5]. Additionally,  $\text{Er}_2\text{O}_3$  has one of the lowest Gibbs free energy of formation among all binary oxide

ceramics [6]. Recently,  $\text{Er}_2\text{O}_3$  is attracting more and more attentions in the application of TPB coatings for fusion systems.

Up to now, we have made rapid progress in the fabrication of TPB coatings by different methods such as sputtering deposition (SD) [7] and metal-organic decomposition (MOD) [8], but complex crystal structures and many surface defects still exist in the coatings, which make it difficult to investigate the detailed mechanism of hydrogen isotope permeation. At present, a high-quality ceramic  $\text{Er}_2\text{O}_3$  thin film with nanostructures is successfully synthesized by arc source plasma assisted deposition (ASPAD). The ceramic shows grain boundary structures which are regarded as large defects in terms of permeation of hydrogen isotopes. Consequently, we place more and more emphasis on investigating hydrogen isotope behavior in this nanostructured thin film because of its slightly simpler structures compared to those prepared by SD and MOD methods.

In addition to experimental studies, *ab-initio* calculations based on density functional theory (DFT) have been applied to complement the established

author's e-mail: mao@nuclear.jp

experimental methods to investigate the energetics and mobility of atomic deuterium (D) in cubic bulk  $\text{Er}_2\text{O}_3$ . In recent years, DFT calculations have become a very valuable tool to elucidate the structures and determine the dynamics of interstitial H in metals, alloys, ceramics and other solids such as heterogeneous catalysts [9]. It is reported that DFT can be used to predict the precise mechanism of H diffusion or reaction events in condensed phases [10]. It is, therefore, essential to apply DFT calculations to the diffusion of hydrogen and its isotopes in  $\text{Er}_2\text{O}_3$  for the verification of experimental data. As a result, a comparison between diffusion experiments and DFT simulations can provide useful information on the mechanism of hydrogen isotope permeation.

In this study, the objective is to compare the diffusion activation energies of interstitial D derived by DFT calculations with the diffusion energy barriers obtained from the experiments, and to study the relationship between the microstructure and hydrogen isotope behavior in  $\text{Er}_2\text{O}_3$  for the mechanism of tritium permeation.

## 2. Methodology

### 2.1. Preparation and characterization of $\text{Er}_2\text{O}_3$ coatings

A mirror polished disk-shaped substrate of 20 mm in diameter and 0.5 mm in thickness was coated by arc source plasma assisted deposition (ASPAD), described in Ref. [7]. The substrate materials were made from reduced activation ferritic/martensitic (RAFM) steels, including JLF-1 (0.10% C; 0.05% Si; 0.45% Mn; 0.003% P; 0.002% S; 0.003% Al; 8.85% Cr; 1.99% W; 0.20% V; 0.080% Ta; 0.0231% N; 0.0002% B; < 0.01% Ni; < 0.05% Cu; < 0.001% Mo; < 0.002% Nb; balance Fe) and F82H (7.65% Cr; 2.00% W; 0.50% Mn; 0.20% V; 0.04% Ta; 0.10% Si; 0.10% C; balance Fe) steels.  $\text{Er}_2\text{O}_3$  coating about  $1.3 \mu\text{m}$  thick was deposited on one side of the substrate. Subsequently, deuterium permeation through the coated sample was carried out in the temperature range 573-973 K at driving pressures of  $10^3$ - $10^5$  Pa [7].

### 2.2. *Ab initio* density-functional calculations in bulk $\text{Er}_2\text{O}_3$

At room temperature,  $\text{Er}_2\text{O}_3$  exhibits cubic rare-earth bixbyite (C phase, space group  $Ia\bar{3}$ ) structure with a large complex unit cell comprising 16  $\text{Er}_2\text{O}_3$  sesquioxide units with an experimental lattice parameter of 1.0543 nm [11]. In this structure, the O anions approximately occupy three-quarters of all the tetrahedral interstices while the Er cations lie in a face centred cubic arrangement. Apart from rotation symmetry, the bixbyite structure is different from that of the fluorite in missing one-fourth of the sites in the anion sublattice in the  $\langle 111$

$\rangle$  direction. That is, it possesses two vacancies (16c) at the corners of the oxygen cube, as shown in Fig. 1.

*Ab initio* density-functional calculations are used to investigate the diffusion behavior of interstitial deuterium in bulk  $\text{Er}_2\text{O}_3$ . We employ Vienna *ab initio* Simulation Package (VASP) for our total energy and DFT calculations. All calculations were performed using the full-potential frozen-core all-electron projected augmented wave (PAW) method within the Generalized Gradient Approximation (GGA) of Perdew and Wang (PW91), as implemented in VASP [12]. The cut-off energy of plane wave was set to 500.0 eV. According to the Monkhorst-Pack scheme [13], we performed the tests with the k-point grid of  $2 \times 2 \times 2$  in the integration over the Brillouin zone. In the initial configuration of the crystal lattice, we have chosen the experimental cubic structure of  $\text{Er}_2\text{O}_3$  unit cell with  $a = 1.0543 \text{ nm}$ , 32 erbium atoms (occupying the 8a and 24d equipoints) and 48 oxygen atoms (occupying 48e equipoints). We conducted *ab initio* DFT calculations in the unit cell of  $\text{Er}_2\text{O}_3$  for the geometry optimization of lattice parameters and atom positions. The geometry relaxations were terminated when residual forces on each atom and energy changes on each atom were less than  $0.001 \text{ eV/\AA}$  and  $1 \times 10^{-5} \text{ eV}$ , respectively. All calculations below referring to interstitial D were performed by inserting an individual D into the cell optimized by DFT methods. It is worth noting that the parameters of cut-off energies and k-point meshes were tested under the convergence criteria of energy changes on each atom less than 0.001 eV, and found sufficient to give reliable convergent results in the *ab initio* DFT calculations.

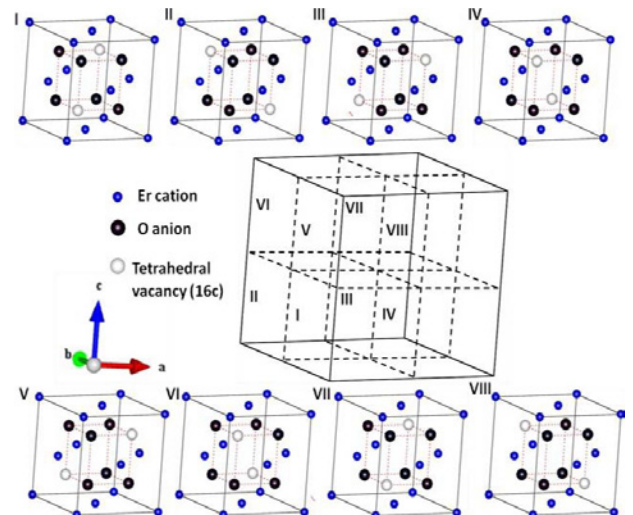


Fig. 1. Cubic bixbyite structure of  $\text{Er}_2\text{O}_3$  unit cell. The cell is subdivided into eight small units, in which tetrahedral vacancies (16c) are virtually depicted as obtained from a comparison between the bixbyite and fluorite structures.

## 3. Results and discussions

### 3.1 Microstructures of $Er_2O_3$ coatings

$Er_2O_3$  coatings of  $1.3 \mu\text{m}$  in thickness were prepared using JLF-1 substrate and the ASPAD method. The coatings were found to possess a high-quality grain boundary nanostructure, as shown in Fig. 2. This grain boundary is regarded as the largest defect because of almost complete absence of other defects such as vacancies and dislocations. The average grain size of the coatings is about 200 nm.

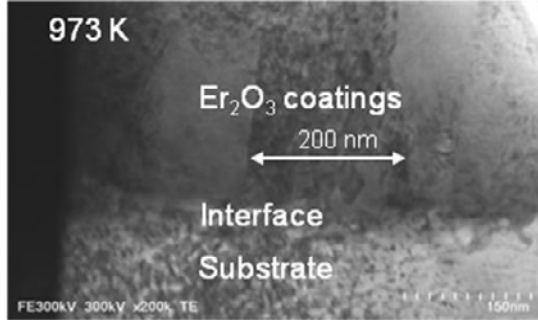


Fig. 2. STEM image of the  $Er_2O_3$  coating fabricated by arc sputtering plasma assisted deposition (ASPAD) at room temperature and annealed at 973 K.

Given no change of grain sizes with instant increase of temperatures, the relationship between grain size and deuterium permeation flux was investigated in the  $Er_2O_3$  coatings by permeation measurements carried out at 773, 873, and 973 K, as shown in Fig. 3. The average grain sizes of the coatings as deposited, after the measurements at 773, 873, and 973 K are 20, 90, 250, and 280 nm, respectively. Apparently, the deuterium permeation flux decreases with increasing grain size when the temperatures are kept constant, in good agreement with previous results [14]. In other words, a decrease of grain sizes results in an increase of the permeation flux of deuterium through the  $Er_2O_3$  coatings.

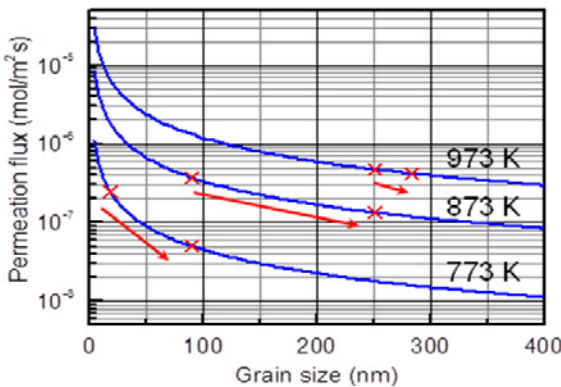


Fig. 3. Grain size dependence of deuterium permeation flux through the  $1.3 \mu\text{m}$  thick  $Er_2O_3$  coatings. The grain sizes of the coatings were estimated by TEM images. The permeation measurements were carried out at a pressure of  $8.00 \times 10^{-4}$  Pa. In the figure, X is the permeation flux-grain size point in the plot, and the red rash arrows represent the change at constant temperatures of 773, 873, and 973 K.

### 3.2 Calculations of $Er_2O_3$ lattice constant

As initial configuration we have selected the experimental cubic structure of  $Er_2O_3$  with a lattice constant of 1.0543 nm. The lattice parameter corresponds to a volume of  $1.1719 \text{ nm}^3$ . After relaxations of the structure with a different lattice constant approaching the experimental one (forces on atoms are less than  $0.001 \text{ eV/\AA}$ ), we obtained the cubic unit cell with a series of values of lattice constant and corresponding volume as a function of total energy shown in Fig. 4. After fitting with Birch-Murnaghan 3rd-order equation of state (EOS) [15], we obtained the balanced volume of  $1.1727 \text{ nm}^3$  corresponding to the lowest total energy and the optimized lattice constant equal to 1.0545 nm, in good agreement with the experimental ones [11].

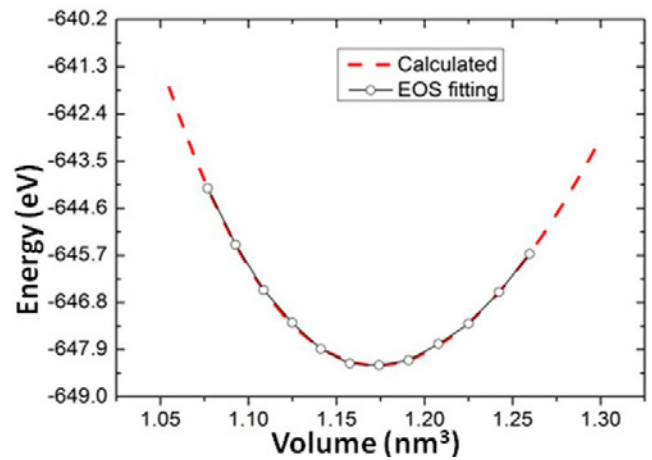


Fig. 4. Total energy configurations as a function of volume in the unit cell of  $Er_2O_3$ . The configurations are performed by ab initio calculations and Birch-Murnaghan 3rd-order EOS fitting.

### 3.3 Individual D atom in bulk $Er_2O_3$

In the lattice model described in Section 2.2, we theoretically occupied the initial positions of tetrahedral vacancies in the oxygen anion sublattice, based on a comparison of the fluorite and bixbyite structures. After relaxing the cell consisting of two primitive units, we introduced an individual neutral hydrogen atom into the cubic bixbyite structure to simulate dilute loadings of interstitial D, and calculate directly its motion by DFT. Considering a great number of interstitial sites (the tetrahedral vacancies of oxygen anion are included) in the structure, we found that D binding energy is mainly dependent on the type of the surrounding atoms, especially the nearest neighboring ones. The binding energy of an interstitial D atom in host lattice can be defined as follows:

$$E_{bind} = E_{(D/S)} - E_{(S)} - E_{(D)} \quad (1)$$

where  $E_{(D/S)}$  and  $E_{(S)}$  are the total energy of the system with and without an interstitial D atom, respectively.  $E_{(D)}$  is the energy of D atoms in free space with spin polarization. With regard to the DFT calculations, the D binding energy

in the tetrahedral vacancies of oxygen anion sublattice were found to be strongest among the interstitial sites, equal to -10 kJ/mol representing an exothermic reaction. This indicates that an individual interstitial deuterium atom is easily trapped in the tetrahedral vacancies. In other words, the tetrahedral interstitial site of oxygen anion sublattice belongs to the local minima position surrounded by the interstitials filled with O anions.

It is worthwhile to look into the effect of spin polarization because the total energy goes down 14~18 kJ/mol when a deuterium atom is inserted into the interstitial site of the tetrahedral. We therefore include spin polarization in the present computational scheme and apply it to an individual H<sub>2</sub> molecule. The calculated binding energy / cohesive energy and bond length of H<sub>2</sub> are 4.55 eV and 0.740 Å, corresponding well to the experimentally obtained values of 4.48 eV and 0.741 Å [16], respectively. Such calculations confirm the fact that the computational scheme considering spin polarization is reliable and sufficient to give fully converging results.

### 3.4 Diffusion behavior of deuterium in bulk Er<sub>2</sub>O<sub>3</sub>

To investigate the diffusion behavior of deuterium in bulk Er<sub>2</sub>O<sub>3</sub>, we employed the DFT calculations to examine trapping binding sites, diffusion pathways and diffusion activation energies for an individual D atom hopping from one local minima position to its nearest neighboring site. The diffusion activation energies ( $E_a$ ) were determined by the energy difference between the local minima position and the activated state site. The hopping distance between the two energy minima in the bulk Er<sub>2</sub>O<sub>3</sub> was measured to be 3.787 Å. The activated states were found by the nudged elastic band (NEB) [17] method using nine images as well as the symmetry consideration, in which forces on atoms are zero and any infinitesimal change of deuterium initial coordinate causes a finite change of atomic coordinates. The identical position of the activated states lies in the Er layer at the point equidistant from Er cations, derived by the above two methods.

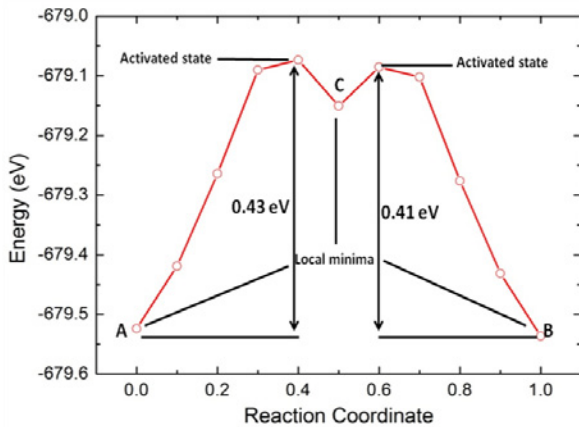


Fig. 5. Energy versus reaction coordinate obtained by the NEB method in bulk Er<sub>2</sub>O<sub>3</sub>. The initial separation distance between the two local minima sites is 3.787 Å.

The overall minimum energy pathway (MEP) shown in Figure 5 indicates another new local minima position (C) and barriers (A-C\*, C-B\*) along the path connecting the initial local minima position (A) and its crystallographic equivalent position (B). The migration barriers from A to C and from C to B are 41.5 kJ/mol (0.43 eV) and 39.6 kJ/mol (0.41 eV), respectively. Furthermore, we have as well calculated a migration barrier of 157.3 kJ/mol (1.63 eV) in the minimum energy pathway of deuterium diffusion along the direction from C to C's crystallographic equivalent site. The maximum (157.3 kJ/mol) in the MEPs corresponds to the position where D diffuses through the highest number of bond making/breaking events in Er<sub>2</sub>O<sub>3</sub>, in which the corresponding activated state locates the O-layer at the site equidistant from O anions.

### 3.5 Relationship between diffusion and permeation of hydrogen and its isotopes through erbium oxide

The permeability of hydrogen isotopes is generally defined as the steady state diffusional transport of atoms through a material supporting a pressure difference. According to the theory reported in the paper of Marchi *et al.* [18], the permeability and diffusivity of hydrogen isotopes through single-layer material can be expressed in the general form as follows:

$$\Phi = \Phi_0 \exp\left(-\frac{E_\Phi}{RT}\right) \quad (2)$$

$$D = D_0 \exp\left(-\frac{E_D}{RT}\right) \quad (3)$$

where  $\Phi$  (mol/m/s/Pa<sup>1/2</sup>) and  $D$  (m<sup>2</sup>/s) are the permeability and diffusivity of hydrogen, respectively.  $R$  (8.314 J/mol/K) is the gas constant;  $T$  (K) is the sample temperature; and  $E_\Phi$  (J/mol) and  $E_D$  (J/mol) are the activation energy of permeation and diffusion of hydrogen and its isotopes, respectively.  $\Phi_0$  and  $D_0$  are the corresponding coefficients of diffusion and permeation. Equations (2) and (3) indicate that diffusivity can represent permeability to a large extent since they are similar in magnitude over a wide range of temperatures in the transport of hydrogen and its isotope atoms through the material.

According to Ref. [14], the permeation flux under steady-state conditions through a single layer barrier can be expressed as

$$J = KD \frac{P^{1/2}}{d} \quad (4)$$

where  $J$  is the permeation flux per unit area of material of thickness  $d$  (m);  $K$  is the Sieverts' constant and  $P$  the driving pressure of hydrogen and its isotopes. Since  $\Phi = KD$ , Eq. (4) in combination with Eq. (2) gives the relationship between the permeation flux ( $J$ ) and the activation energy ( $E_D$ ) of diffusion under steady-state conditions, i.e.

$$J = \Phi P^{1/2} / d = \Phi_o \exp\left(-\frac{E_D + E_S}{RT}\right) P^{1/2} / d \quad (5)$$

where  $E_s$  (J/mol) is the heat of solution of hydrogen atoms in the single-layer material or oxide with a thickness of  $d$  (m), and  $E_\phi$  is defined as the sum of  $E_S$  and  $E_D$ . It is obvious that diffusion plays an important role in the process of permeation of hydrogen and its isotopes based on the relationship of permeation flux  $J$  and diffusion activation energy  $E_D$  given in Eq. (5). With the aim of understanding the mechanism of permeation it is therefore reasonable to study first the diffusion behavior of hydrogen and its isotopes through erbium oxide.

In experiments on the permeation of deuterium, the diffusion activation energy was estimated from an Arrhenius plot of temperature versus diffusivity,  $D$  being obtained by measuring the time-lag  $t_l$  (s) with relationship  $t_l$  (s) =  $d^2/6D$ , as described in [19]. The measured activation energy of approximate 20.0 kJ/mol [14] is of similar order of magnitude with the D diffusion energy barrier of 157.3 kJ/mol evaluated by the NEB method as implement in *ab initio* DFT calculations. The discrepancy in activation energies is partly attributed to the fact that nanostructured  $\text{Er}_2\text{O}_3$  thin films were used in the experiments while bulk  $\text{Er}_2\text{O}_3$  was adopted in the computational simulations. Although the  $\text{Er}_2\text{O}_3$  thin films were prepared by the ASPAD method with the aim of achieving good performance as TPB coatings, they had very large defects, i.e. grain boundaries (GB's) within the nanostructure as revealed by Fig. 1. A GB represents an environment where the symmetry of a crystal is terminated. Apart from the diffusion of hydrogen and its isotopes through the bulk of erbia, diffusion is likely to occurs also via the large defect GB's.

In order to elucidate the hydrogen behavior in erbium oxide, we purposely conducted *ab initio* DFT calculations in the bulk  $\text{Er}_2\text{O}_3$  assuming an ideal crystal structure. The volume and geometry relaxations in the calculations show that an individual interstitial D prefers to bind in the tetrahedral interstitial sites of O anion sublattice (local minima). MEP found by the NEB method shows the diffusion pathway of deuterium hopping from one local minima to the nearest neighboring one. Most important, the maximum energy difference between the minimum site and the estimated transition state (saddle point) determined in this way is 157.3 kJ/mol, and somewhat higher than the experimental value of 20.0 kJ/mol. This indicates that at the grain boundary the activation energy for hydrogen isotope (deuterium) diffusion decreases because of the different diffusion pathway as predicted by MEP. In other words, the diffusivity of deuterium will be increased if we introduce GB into the perfect bulk  $\text{Er}_2\text{O}_3$ . On the basis of Eq. (5), which relates the permeation flux  $J$  to the diffusivity  $D$ , the permeability will increase

correspondingly. Actually, GB's existing in  $\text{Er}_2\text{O}_3$  coatings degrade the grain sizes due to loss of bulk area and lead to an increase of permeation flux, in good agreement with the experimental data given in Fig. 3. It is intuitively considered that diffusion and permeation of hydrogen and its isotopes through erbium oxide are likely to occur predominately through grain boundaries rather than grains. In addition, it is worth noting that the activation energy obtained in the deuterium permeation is still large and high concentration to that derived by the DFT calculations. This suggests that the  $\text{Er}_2\text{O}_3$  coatings prepared by the ASPAD method possess high performance as required for TPB coatings. As shown in Fig. 3, the growth of grain size enhances the ability of the coatings to suppress deuterium diffusion and permeation. As the grains become very large, the permeability of deuterium will decrease because of the absence of grain boundaries. That is, the activation energy is maximized when the  $\text{Er}_2\text{O}_3$  coatings become a perfect crystal without any grain boundary as assumed in the DFT calculations.

#### 4. Conclusions

In this study, the mechanism of tritium permeation through  $\text{Er}_2\text{O}_3$  has been investigated by the experimental measurements and the computational simulations. We have prepared  $\text{Er}_2\text{O}_3$  coatings of 1.3  $\mu\text{m}$  in thickness by the ASPAD method and characterized the coatings via deuterium permeation measurements. From the experiments, we concluded that a grain boundary nanostructure exists in the  $\text{Er}_2\text{O}_3$  coating and estimated the diffusion activation energy to be 20.0 kJ/mol. Additionally, *ab initio* DFT calculations based on transition state theory were carried out for interstitial deuterium in an ideal supercell assuming cubic bixbyite  $\text{Er}_2\text{O}_3$ . Calculated and fitted lattice constants of  $\text{Er}_2\text{O}_3$  showed good agreement with the experimental data. Also the minimum energy sites, diffusion pathways and diffusion activation barriers for an individual D atom were found by MEP calculations. The local minima position is found located in the tetrahedral interstitial site of oxygen anion sublattice. The results indicate that the preferred hopping path of individual D atoms is from one local minima position to its nearest neighboring site. The maximum diffusion activation energy resulting from the MEP calculation is 157.3 kJ/mol and higher than that obtained experimentally (20.0 kJ/mol). This discrepancy is attributed to grain boundary structures found in the  $\text{Er}_2\text{O}_3$  coatings. GB's lead to pathways of hydrogen diffusion different from MEP derived by DFT calculations. They provide useful information on tritium permeation mechanism in erbium oxide. Additionally, it appears that diffusion and permeation of hydrogen and its isotopes through the  $\text{Er}_2\text{O}_3$  coatings will probably take place through grain boundaries rather than grains. This

conclusion is drawn from *i*) the comparison of the activation energy between diffusion experiments and DFT simulations *ii*) the interdependence of hydrogen and its isotope diffusion and permeation, and *iii*) the relationship between the permeation flux and grain size during the measurement of deuterium permeation.

### Acknowledgements

This work was supported in part by GoNERI, the Global Center of Excellence (G-COE) Program of the Nuclear Education and Research Initiative of the Japan Society for the Promotion of Sciences (JSPS).

### References

- [1] V.A. Maroni, Tritium Processing and Containment Technology for Fusion Reactors: Perspective and status, Proc. Second Topical Meeting on the Technology of Controlled Nuclear Fusion, USERDA Report CONF -760935-P3 (1976) P. 799.
- [2] F. N. Flakus, At. Energy Rev. **13**, 587 (1975).
- [3] G.W. Hollenberg, E.P. Simonen, G. Kalinin, A. Terlain, Fusion Eng. Des. **28**, 190 (1995).
- [4] Z. Yao, A. Suzuki, D. Levchuk, T. Chikada, T. Tanaka, T. Muroga, T. Terai, J. Nucl. Mater. **386-388**, 700 (2009).
- [5] Z. Yao, A. Suzuki, T. Muroga, K. Katahira, J. Nucl. Mater. **329-333**, 1414 (2004).
- [6] MATL2 (Materials oriented Little Thermodynamic database 2), Version 1.06, The Japan Society of Calorimetry and Thermal Analysis ( Kagaku Gijutsu Sha, Japan, 1992).
- [7] T. Chikada, A. Suzuki, Z. Yao, A. Sawada, T. Terai, T. Muroga, Fusion Eng. Des. **82**, 2572 (2007).
- [8] T. Chikada, A. Suzuki, T. Tanaka, T. Terai, T. Muroga, Fusion Eng. Des. **85**, 1537 (2010).
- [9] K. Honkala, A. Hellman, I.N. Remediakis, Á. Logadóttir, A. Carlsson, S. Dahl, C.H. Christensen, J.K. Nørskov, Science **507**, 555 (2005).
- [10] D.S. Sholl, J. Alloy. Compd. **446-447**, 462 (2007).
- [11] Y.E. Bogatov, A.K. Molodkin, M.G. Safronko, Y.Y. Nevyadomskaya, Russ. J. Inorg. Chem. **39**, 211 (1994).
- [12] G. Kresse, J. Furthmuller, Phys. Rev. B **54**, 11169 (1996).
- [13] H.J. Monkhorst, J.D. Pack, Phys. Rev. B **13**, 5188 (1976).
- [14] T. Chikada, A. Suzuki, H. Maier, T. Terai, T. Muroga, Fusion Sci. Technol. **60**, 389 (2011).
- [15] F. Birch, Phys. Rev. **71**, 809 (1947).
- [16] B.G. Johnson, P.M.W. Gill, J.A. Pople, J. Chem. Phys. **98**, 5612 (1993).
- [17] H. Jónsson, G. Mills, K. W. Jacobsen, *Classical and Quantum Dynamics in Condensed Phase Simulations*, edited by B. J. Berne, G. Ciccotti and D. F. Coker (World Scientific, Singapore, 1998), pp. 385-404.
- [18] C. San Marchi, B.P. Somerday, S.L. Robinson, Int J Hydrogen Energy, **26**, 597 (2001).
- [19] T. Chikada, A. Suzuki, T. Kobayashi, H. Maier, T. Terai, T. Muroga, J Nucl. Mater. **417**, 1241 (2011).